

Computerised analysis of osteoporotic bone patterns using texture parameters characterising bone architecture

¹H JEONG, PhD, ²J KIM, PhD, ³T ISHIDA, PhD, ⁴M AKIYAMA, MD and ²Y KIM, PhD

¹Department of Radiological Science, Baekseok Culture University, Chungchungnam-do, Republic of Korea, ²Department of Radiologic Science, College of Health Science, Korea University, Seoul, Republic of Korea, ³Department of Medical Physics and Engineering, Division of Health Sciences, Osaka University Graduate School of Medicine, Osaka, Japan, and ⁴Department of Clinical Radiology, Faculty of Health Sciences, Hiroshima International University, Hiroshima, Japan

Objective: To evaluate the geometric change of osteoporotic bone trabecular patterns using root mean square (RMS) values, first moment power spectrum (FMP) values and fractal dimension values. With the use of these methods, we attempted computerised analysis of osteoporotic bone patterns using texture parameters characterising bone architecture and computer-aided diagnosis of osteoporosis.

Methods: 32 patient cases from Korea University Guro Hospital were analysed. Patient ages ranged from 51 to 89 years, with a mean age of 65 years. Receiver operating characteristic curve analysis was performed with determination of the area under the curve (AUC).

Results: The bone mineral density (BMD) measurement (AUC=0.78) was a better indicator of bone quantity than the RMS, FMP and fractal dimension values (AUC=0.72) for diagnosis; therefore the combination of RMS, FMP and fractal dimension values was a better indicator of bone quality.

Conclusion: Measurements that combined BMD measurement and RMS values and combined FMP and fractal dimension values (AUC=0.85) together produced better results than the use of the two parameter sets separately for a diagnosis of osteoporosis.

Advances in knowledge: For more effective application, additional study on more cases and data will be required.

Received 26 November 2010
Revised 17 August 2012
Accepted 3 September 2012

DOI: 10.1259/bjr.20101115

© 2013 The British Institute of Radiology

Osteoporosis is a condition in which the decreases in bone strength and density ultimately lead to fragile bones and subsequent fractures. Osteoporosis has been recognised as an established and well-defined disease that affects >75 million people in USA, Europe and Japan, and causes >4.5 million fractures annually in the USA and Europe [1].

Osteoporosis does not only cause fractures, it also results in elderly subjects becoming bedridden with potentially life-threatening secondary complications. Since osteoporosis also causes back pain and loss of height, prevention of the disease and its associated fractures is essential in order to maintain health, quality of life and independence among the elderly [2].

There are commonly used methods in diagnosing osteoporosis. The most widely utilised method to assess the bone mass is the determination of bone mineral density (BMD). This method is readily available and popular for its non-invasive means to identify osteoporosis in a patient. BMD is only one contributor towards determining bone strength and fracture risk reduction. In fact, BMD by dual-energy X-ray absorptiometry (DXA) is widely used for diagnosing osteoporosis. The World Health Organization (WHO) defines osteoporosis as a BMD that is 2.5 standard

deviations (SD) or more below the mean of a young adult of the same sex (T-score) [3, 4].

Although the use of BMD is becoming much more frequent, there are several key concerns that need to be addressed before this method of diagnosis is undertaken. Routine DXA scanning sporadically identifies individuals with extremely high BMDs, which are not always explained by artefactual causes such as osteoarthritis (OA), the syndesmophytes of ankylosing spondylitis or surgically implanted metalwork. Paget's disease, certain malignancies and rare conditions such as myelofibrosis and hepatitis C osteosclerosis can also raise BMD [5–8].

Heterogeneity of density due to osteoarthritis or a previous fracture can often be detected on a scan, and can sometimes be excluded from the analysis [3]. Because of osteoarthritis, features such as soft-tissue calcification, the presence of overlying metal objects, or the presence of compression fractures and previous fractures, it can be difficult to diagnose osteoporosis using only DXA.

The other diagnostic method for both osteoporosis and the assessment of bone mass is through the use of radiography. In this procedure, the Jikei University classification or Itami index is used [9], which radiographically classifies the stage of bone loss in a vertebral body (Figure 1). Approximately 25% of the vertebral bodies classified as first stage based on the Itami index, 60% of the vertebral bodies classified as second stage and

Address correspondence to: Professor Jungmin Kim, Department of Radiologic Science, College of Health Science, Korea University, 136–703 Seoul, Republic of Korea. E-mail: minbogun@korea.ac.kr
This research was supported by a Korea University Grant.

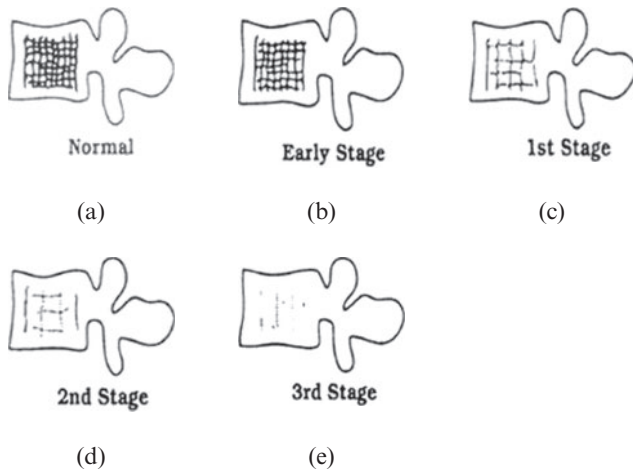


Figure 1. (a) Normal: there are dense trabecular patterns in both the horizontal and vertical direction. (b) Early stage: bone images become lower in clarity and trabeculae become thinner. (c) First stage: trabeculae decrease in the horizontal direction and become more isolated in the vertical direction. (d) Second stage: in the horizontal direction, trabeculae continue to decrease. Also, in the vertical direction, they become thinner. (e) Third stage: trabeculae become distinguishable in both the horizontal and vertical direction. Bone images appear blurred. Scheme and details of the Jikei University classification or Itami index, which classifies radiographically the stage of bone loss in a vertebral body. Source: Itami and Ohata [9].

90% of the vertebral bodies classified as third stage have been reported to have suffered traumatic fractures.

Caligiuri et al [10] previously reported that using computerised radiographic methods to evaluate bone structure, such as fractal analysis, might be more helpful to determine fracture risk in osteoporosis. Takigawa et al [11] quantitatively evaluated trabecular patterns by spectral analysis of the patterns on lateral views of the lumbar vertebrae. Ishida et al [12, 13] evaluated the patterns of power spectra with a two-dimensional fast Fourier transform (2DFFT) and a one-dimensional maximum entropy method (1DMEM). Nishihara et al [14] developed an algorithm that distinguished the central part of the vertebral body using abdominal X-ray CT images in order to determine whether it was possible to aid in the diagnosis of osteoporosis. Dougherty and Henebry [15] reported that the maximum deviation of the lacunarity from a neutral (fractal) model used with bone mineral density may have diagnostic value in characterising osteoporosis and predicting fracture risk. Ito et al [16] reported that vertebral microarchitecture can be visualised through multidetector CT (MDCT), and that microstructure parameters obtained by MDCT, together with volumetric BMD, provide better diagnostic performance for assessing fracture risk than DXA measurement. Recent studies have demonstrated that microarchitectural measurements acquired using high-resolution MDCT imaging available *in vivo* correlate strongly with those assessed using high-resolution peripheral quantitative CT [17, 18].

In this paper, we have attempted to evaluate the geometric change of trabecular patterns using root mean square (RMS), first moment power spectrum (FMP) and fractal dimension.

Materials and methods

Database

We studied 32 patient cases from Korea University Guro Hospital. All patients were post-menopausal females with ages ranging from 51 to 89 years, and the mean age of the group was 65 years. All of the patients who participated in the examination gave their consent.

All patients had already undergone a lumbar spine CT examination within a few months of BMD. 5 of the patients had a normal diagnosis and 12 were diagnosed with osteopenia. The remainder of the patients were diagnosed with osteoporosis. General diagnostic categories that had been proposed by the WHO and modified by the International Osteoporosis Foundation were followed for assessments performed with DXA [1, 2].

Bone densitometry and multidetector CT imaging

The measurements of BMD were determined using a DXA system (Discovery A; Hologic, Bedford, MA). The diagnosis was performed in a standard anterior-posterior projection of the lumbar spine with attention to the L2-L4 levels. The volume measurements of the lumbar vertebra were examined through the use of a 15-slice MDCT scanner (Sensation15; Siemens, Erlangen, Germany). The tube voltage was 120 kVp and the matrix size used was 512×512 pixels. The slice thickness was originally 0.5 mm. This meant that the interval of each slice was 0.5 mm on z-axis. However, the pixel spacing on x, y-axis was 0.25 mm by magnification. Lumbar vertebrae 2-4 were considered appropriate for comparing the CT image with the BMD. The analysis was conducted by BMD without any diagnosed or observed conditions (e.g. surgically implanted metalwork, compression fracture and osteoarthritis) that could be capable of affecting the bone density of the spine.

Processing for regions of interest

Data pertaining to CT volume and sagittal images were reconstructed by using the Jikei University classification (Figure 1). The matrix size for the region of interest (ROI) regarding data input was determined as 64×64 pixels×100 slices (32.0×32.0×50.0 mm; pixel spacing was 0.5 mm). All ROIs were corrected for a non-uniform background trend by using a two-dimensional surface-fitting technique. A background trend correction through the use of a second-order polynomial least-squares fit [19] was performed on the ROIs prior to texture analysis. The purpose of this correction was to remove any trends varying slowly in the image due to variations in bone thicknesses and the anode-heel effect. Subsequently, the Blackman window function [20] was applied to the ROIs. When the frequency image was transformed back to the spatial domain, it contained spatial distortion artefacts because of an edge effect. The edge effect was minimised by using the sampled image in a frequency domain by a window function. The Blackman window function results in poor frequency resolution; however, it can be

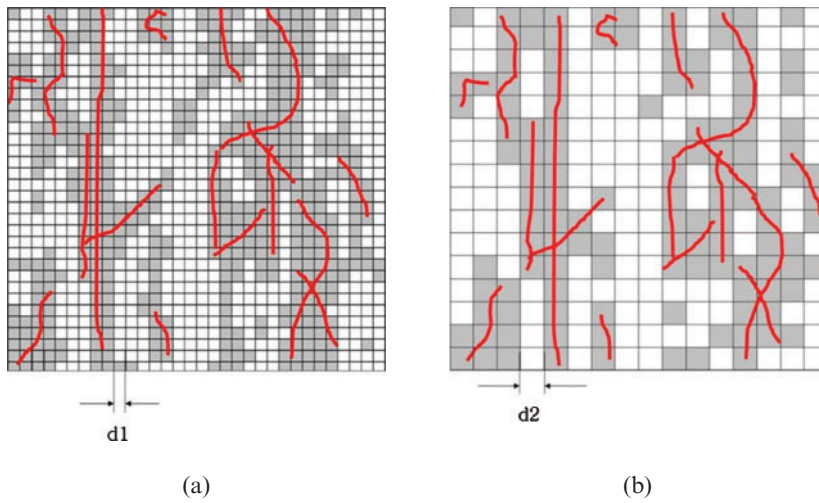


Figure 2. The image was divided into units of dimensions (a) $d1 \times d1$ and (b) $d2 \times d2$ (mesh type), with only shaded units counted. The fractal dimension of the structure regarding the bone trabecular pattern was measured by the box-counting method.

applied in a wide dynamic range because small ROIs (64×64 pixels) of data were used.

Root mean square and first moment of the power spectrum

Fast Fourier transformation was then performed, and the resulting power spectrum was analysed in order to yield the RMS [21]:

$$RMS = \sqrt{\int_{-\infty}^{\infty} \int_{-\infty}^{\infty} |f(\mu, \nu)|^2 d\mu d\nu} \quad (1)$$

The FMP was calculated as:

$$FMP = \frac{\int_{-\infty}^{\infty} \int_{-\infty}^{\infty} \sqrt{\mu^2 + \nu^2} |f(\mu, \nu)|^2 d\mu d\nu}{\int_{-\infty}^{\infty} \int_{-\infty}^{\infty} |f(\mu, \nu)|^2 d\mu d\nu} \quad (2)$$

where $f(\mu, \nu)$ corresponds to the Fourier transform for the background-corrected ROI of the trabecular pattern, and μ and ν are indices of the ROI array [21].

Fractal dimension

When we used the fractal dimension, background trend correction images were used. We placed a structure onto a regular mesh grid and counted the number of boxes that contained some part of the structure, as shown in Figure 2. We changed the mesh size to progressively smaller sizes and counted the corresponding number $N(d)$ (number of units of dimension in Figure 2), the following fractal dimension was obtained [22].

The fractal dimension (D) for each ROI was calculated, using

$$D = 2 - H$$

where H was the slope of a least-squares line fitted to the relationship of log box counting versus log pixel size for

each ROI. The number 2 is the topological dimension of the grey-level surface.

Binarisation was conducted by using a threshold that distinguished bone texture from soft tissue and fat. We changed the threshold from 0 to 50, and analysed the correlation between fractal dimension and SD for the fractal dimension. It demonstrated an increased threshold from 0 to 30. It was highest at a threshold of 30; however, it decreased over a threshold of 40. Owing to these results, we applied our analysis at a threshold of 30 for all data.

Figure 3 shows a schematic diagram of the RMS, FMP and fractal dimension.

Receiver operating characteristic analysis

The ability of a fractal dimension to distinguish between fracture cases was evaluated by using a receiver operating characteristic (ROC) curve analysis. Using the fractal dimension was compared with the performance of BMD in patients diagnosed with osteoporosis. The ROC curves were derived by using the LABROC program,

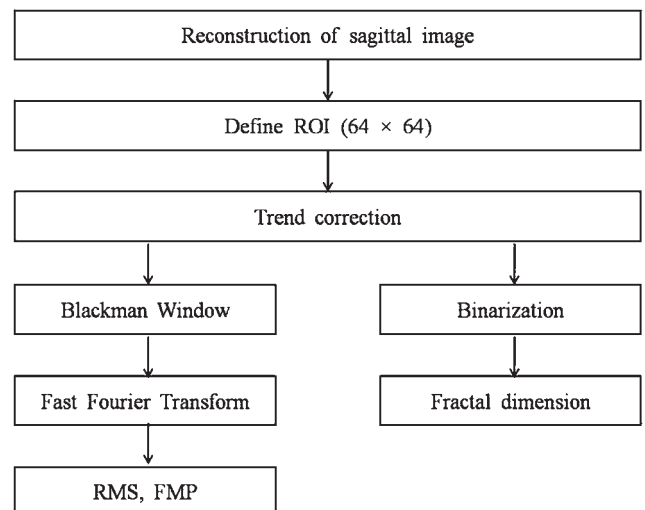


Figure 3. Schematic diagram of root mean square (RMS), first moment power spectrum (FMP) and fractal dimension. ROI, region of interest.

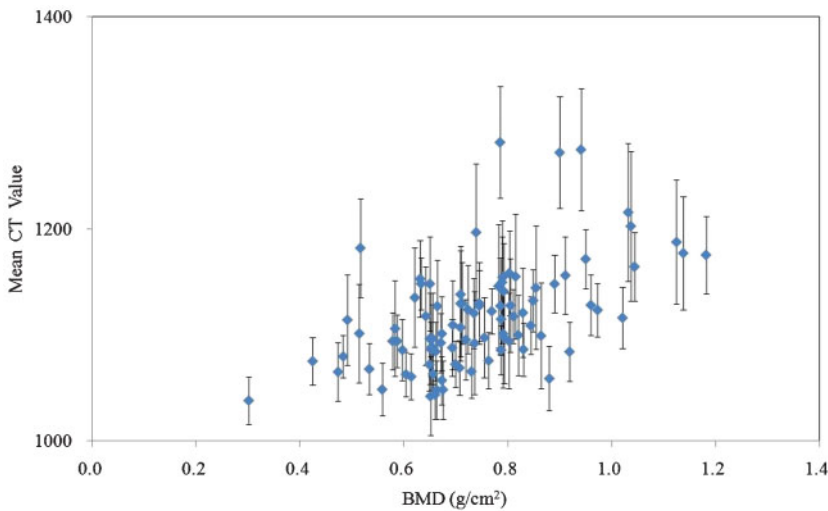


Figure 4. Relationship between bone mineral density (BMD) and mean CT number. There was a weak positive correlation for Pearson’s correlation coefficient of $R^2=0.30$, statistically significant at the $p<0.01$ level.

which required input in the form of values for actual negative cases (*i.e.* cases without a fracture elsewhere in the spine) and values for actual positive cases (*i.e.* cases with a fracture elsewhere in the spine). This program computed the area under the ROC curve (AUC); the greater the AUC, the better the performance for the measurement of the specific task (to distinguish cases with osteoporosis from cases without osteoporosis).

Results

Figure 4 illustrates the relationship between BMD and the mean CT number (the distribution of the photon’s linear-attenuation coefficients in the meter [23]). The range for CT numbers was 1190.66 ± 51.6 HU (Hounsfield units) in the normal group, 1120.3 ± 26.2 HU in the osteopenia group and 1086.9 ± 29.8 HU in the osteoporosis C group.

Figure 5 illustrates the relationship between BMD and RMS values. The range of the RMS was 32.8 ± 10.8 in the normal group, 28.3 ± 8.4 in the osteopenia group and 23.3 ± 7.1 in the osteoporosis group.

Figure 6 illustrates the relationship between BMD and FMP values. The range of the FMP was 0.32 ± 0.14 in the normal group, 0.30 ± 0.06 in the osteopenia group and 0.27 ± 0.05 in the osteoporosis group.

Figure 7 illustrates the relationship between BMD and fractal dimension values. The range for the fractal dimension values was 2.654 ± 0.017 in the normal group, 2.658 ± 0.017 in the osteopenia group and 2.662 ± 0.028 in the osteoporosis group.

All data indicated a weak positive correlation for the BMD and mean CT number, and showed no tendency for the BMD and RMS. However, the data seemed to be classified significantly into two groups—BMD-FMP and BMD-RMS.

Higher RMS was accompanied by an increase in the values regarding the RMS SD. The RMSs were divided into two groups; one group was for a high RMS and the other group was for a low RMS value. The cause of separation was the RMS and its SD (Figure 8). Discriminant analysis was performed using R v. 2.7 statistical software [24].

The discriminant for the high-RMS group and the low-RMS group was:

$$y = 0.63x - 13.77$$

The low-RMS group indicated a moderate negative correlation between the RMS and its SD. However, the high-RMS group indicated no linear correlation between

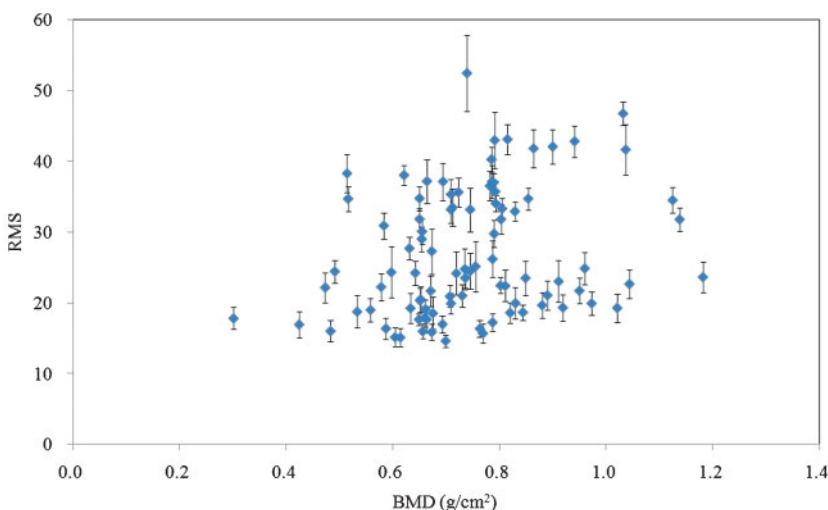


Figure 5. Relationship between bone mineral density (BMD) and mean square (RMS) values. There was no correlation for Pearson’s correlation coefficient of $R^2=0.07$, statistically significant at the $p<0.01$ level.

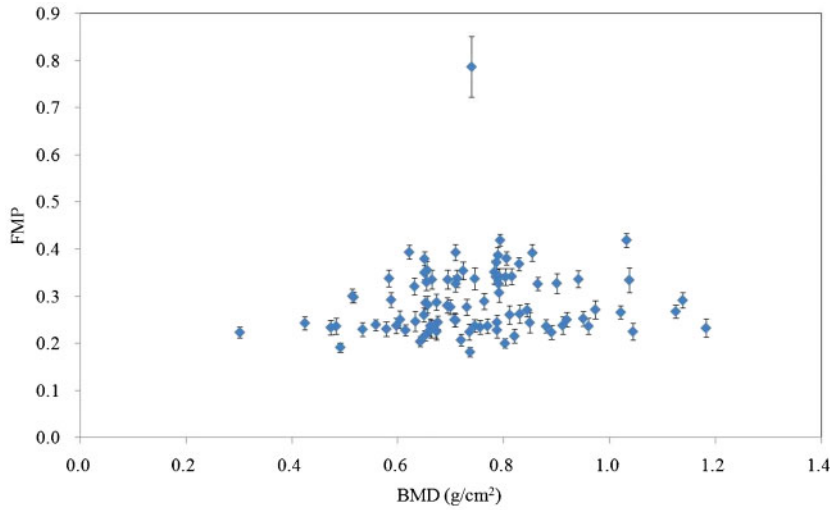


Figure 6. Relationship between bone mineral density (BMD) and first moment power spectrum (FMP) value. There was no correlation for Pearson's correlation coefficient of $R^2=0.01$, statistically significant at the $p<0.01$ level.

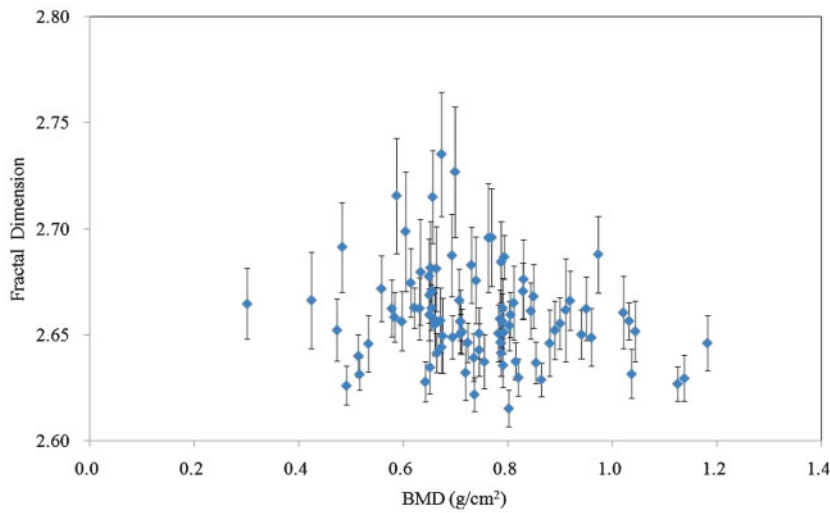


Figure 7. Relationship between bone mineral density (BMD) and fractal dimension value. There was no correlation for Pearson's correlation coefficient of $R^2=0.05$, statistically significant at the $p<0.01$ level.

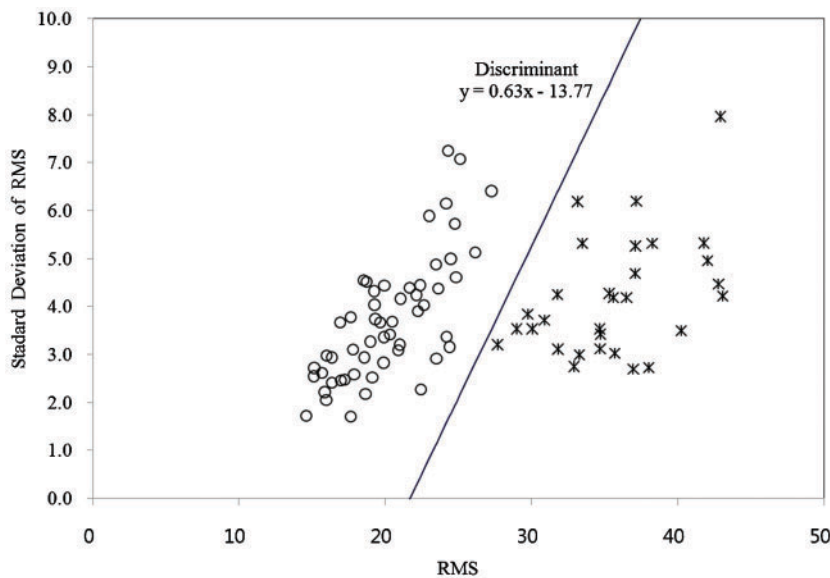


Figure 8. Relationship between the root mean square (RMS) and its standard deviation. The low-RMS group had a moderate negative correlation, with Pearson's correlation coefficient of $R^2=0.54$. The high-RMS group did not linearly correlate with Pearson's correlation coefficient of $R^2=0.19$, statistically significant at the $p<0.01$ level. Circle, low-RMS group; star, high-RMS group.

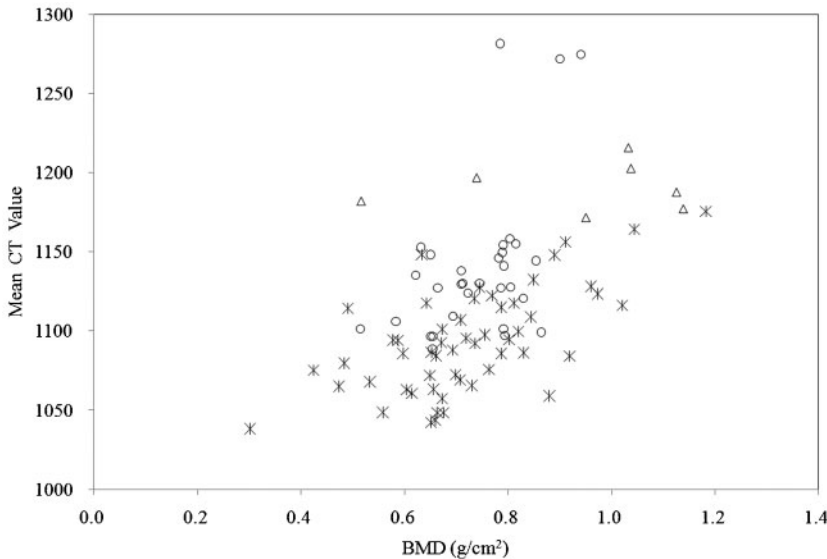


Figure 9. Second analysis for the relationship between the bone mineral density (BMD) and mean CT number. The low-root mean square (RMS) group indicated weak positive correlation, with Pearson's correlation coefficient of $R^2=0.40$. The high-RMS group indicated weak positive correlation, with Pearson's correlation coefficient of $R^2=0.27$, statistically significant at the $p<0.01$ level. Circle, low-RMS group; star, high-RMS group; triangle, fracture.

the RMS and its SD. Data from Figures 4-7 were recategorised by using two RMS groups separated in Figure 8.

The low-RMS group indicated a weak positive correlation with Pearson's correlation coefficient of $R^2=0.40$. The high-RMS group also indicated a weak positive correlation with Pearson's correlation coefficient of $R^2=0.27$, statistically significant at the $p<0.01$ level (Figure 9). Although there was not a strong positive correlation on either the low-RMS group or the high-RMS group, osteoporosis seemed to be generally associated with decreased mean CT number.

The low-RMS group and the high-RMS group indicated no linear correlation between BMD and RMS, with Pearson's correlation coefficients of $R^2=0.21$ and $R^2=0.08$, respectively, statistically significant at the $p<0.01$ level. Both the low-RMS group and the high-RMS group demonstrated no correlation between BMD and RMS (Figure 10).

The low-RMS group and the high-RMS group showed no linear correlation between BMD and FMP, with Pearson's correlation coefficients of $R^2=0.01$ and

$R^2=0.02$, respectively, statistically significant at the $p<0.01$ level (Figure 11).

Both the low-RMS group and the high-RMS group were not influenced by the BMD and fractal dimension (Figure 12). The range of fractal dimension in the low-RMS group was 2.661 ± 0.016 in the normal group, 2.664 ± 0.018 in the osteopenia group and 2.665 ± 0.031 at the osteoporosis group. The range of fractal dimension in the high-RMS group was 2.654 ± 0.004 in the normal group, 2.654 ± 0.014 in the osteopenia group and 2.655 ± 0.010 in the osteoporosis group.

Figure 13 illustrated the relationship between RMS and FMP. The results of the high-RMS group and the low-RMS group were clearly separated by each group in this figure. The low-RMS group indicated weak negative correlation between RMS and FMP, with Pearson's correlation coefficient of $R^2=0.26$. The high-RMS group indicated no correlation between RMS and FMP, with Pearson's correlation coefficient of $R^2=0.03$, statistically significant at the $p<0.01$ level.

Figure 14 illustrates the relationship between RMS and fractal dimension. The separation for the high-RMS group

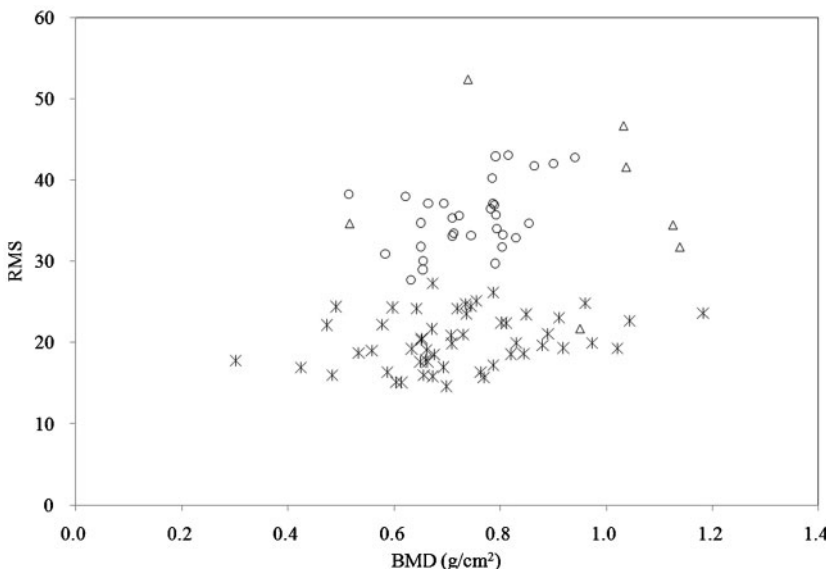


Figure 10. Second analysis for the relationship between bone mineral density (BMD) and root mean square (RMS). The low-RMS group and the high-RMS group showed no linear correlation with respect to RMS and BMD, with Pearson's correlation coefficients $R^2=0.21$ and $R^2=0.08$, respectively, statistically significant at the $p<0.01$ level. Circle, low-RMS group; star, high-RMS group; triangle, fracture.

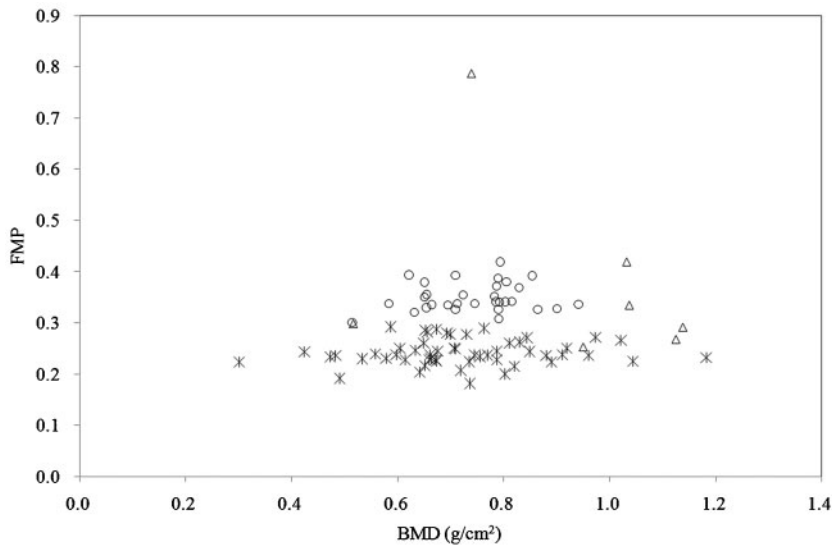


Figure 11. Second analysis regarding the relationship between the bone mineral density (BMD) and first moment power spectrum (FMP). The low-root mean square (RMS) group and the high-RMS group showed no linear correlation between BMD and FMP, with Pearson's correlation coefficients of $R^2=0.01$ and $R^2=0.02$, respectively, statistically significant at the $p<0.01$ level. Circle, low-RMS group; star, high-RMS group; triangle, fracture.

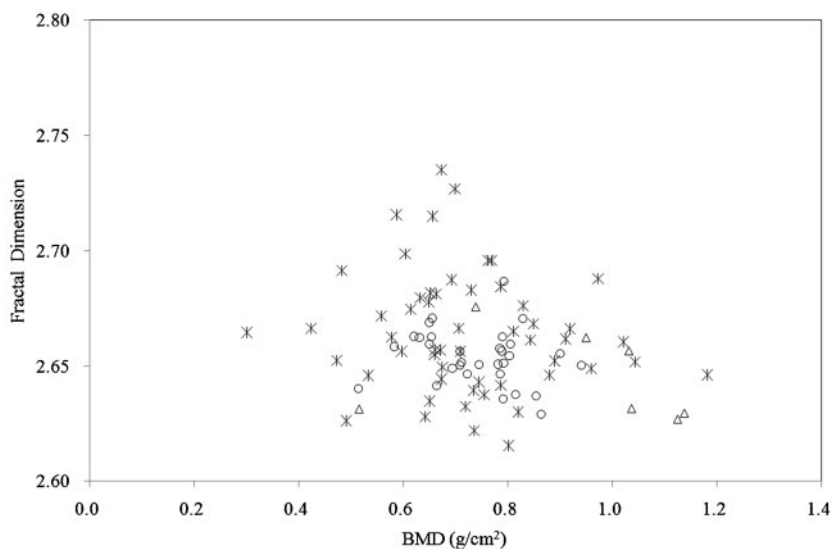


Figure 12. Second analysis regarding the relationship between bone mineral density (BMD) and the fractal dimension. The low-root mean square (RMS) group and the high-RMS group were not clearly distinguished in this figure. The second analysis did not show any linear correlation between BMD and the fractal dimension, with Pearson's correlation coefficient of $R^2=0.02$ in the low-RMS group and $R^2=0.03$ in the high-RMS group, statistically significant at the $p<0.01$ level. Circle, low-RMS group; star, high-RMS group; triangle, fracture.

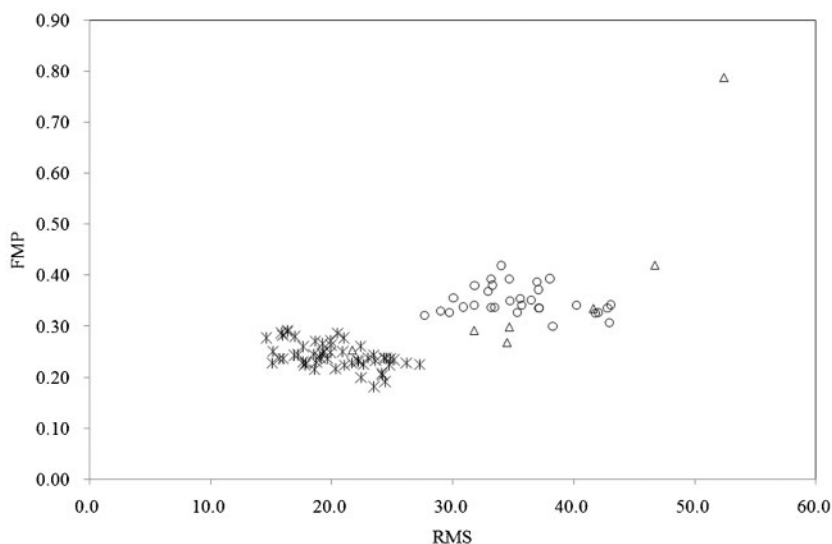


Figure 13. Relationship between root mean square (RMS) and first moment power spectrum (FMP). The low-RMS group showed weak negative correlation, with Pearson's correlation coefficient of $R^2=0.26$. The high-RMS group showed no correlation, with Pearson's correlation coefficient of $R^2=0.03$, statistically significant at the $p<0.01$ level. Circle, low-RMS group; star, high-RMS group; triangle, fracture.

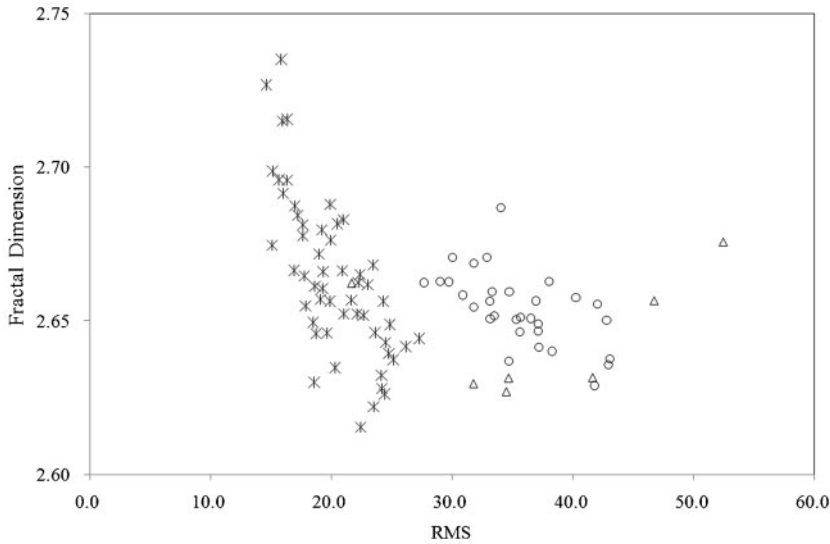


Figure 14. Relationship between root mean square (RMS) and fractal dimension. The low-RMS group demonstrated a moderate negative correlation, with Pearson's correlation coefficient of $R^2=0.53$. The high-RMS group showed a weak negative correlation, with Pearson's correlation coefficient of $R^2=0.35$, statistically significant at the $p<0.01$ level. Circle, low-RMS group; star, high-RMS group; triangle, fracture.

and the low-RMS group can be easily distinguished in this figure. The low-RMS group demonstrated moderate negative correlation with Pearson's correlation coefficient of $R^2=0.53$. The high-RMS group showed weak negative correlation with Pearson's correlation coefficient of $R^2=0.35$, statistically significant at the $p<0.01$ level.

Figure 15 illustrates the relationship between FMP and fractal dimension. The low-RMS group showed a moderate positive correlation with Pearson's correlation coefficient of $R^2=0.66$. The high-RMS group showed a weak positive correlation with Pearson's correlation coefficient of $R^2=0.23$, statistically significant at the $p<0.01$ level.

Discussion

CT data analysis resulted in several key points. Analysed data from Figures 4 and 5 showed that BMD had a weak positive correlation with mean CT number and RMS. However, BMD had no correlation with FMP and fractal dimension (Figures 6 and 7).

In BMD-RMS, the data had a tendency to be classified into two groups: the higher group and the lower group, based on RMS. A similar tendency was also shown by BMD-FMP. By additional analysis, it was indicated that all RMS data were classified into two groups: a high-RMS group and a low-RMS group by the RMS and its SD (Figure 8).

It was not an effective method for evaluating BMD by using mean CT number only (Figure 9). Both the low-RMS group and the high-RMS group had weak correlation between mean CT number and BMD. Osteoporosis seemed to be generally associated with decreased mean CT number.

The BMD-RMS, BMD-FMP, and BMD-fractal dimension did not show the same tendency (Figures 5, 6 and 12). However, in all these cases, data were separated into a high-RMS group and a low-RMS group clearly.

Osteoporosis was indicated as the increase of both fractal dimension and its SD (Figures 7 and 12). A strong correlation was found in RMS-FMP and RMS-fractal dimension (Figures 13 and 14). In this case, a larger SD indicated that osteoporosis was in progress. When

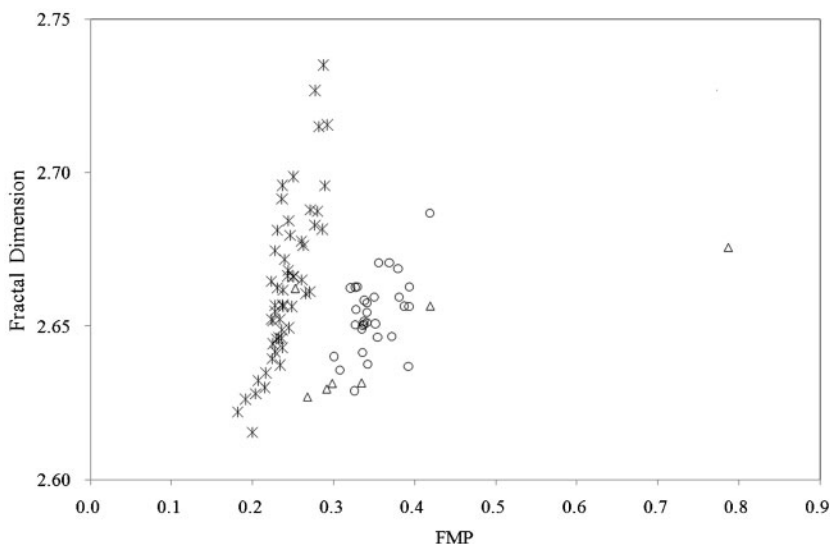


Figure 15. Relationship between first moment power spectrum (FMP) and fractal dimension. The low-root mean square (RMS) group showed a moderate positive correlation, with Pearson's correlation coefficient of $R^2=0.66$. The high-RMS group showed weak positive correlation, with Pearson's correlation coefficient of $R^2=0.23$, statistically significant at the $p<0.01$ level. Circle, low-RMS group; star, high-RMS group; triangle, fracture.

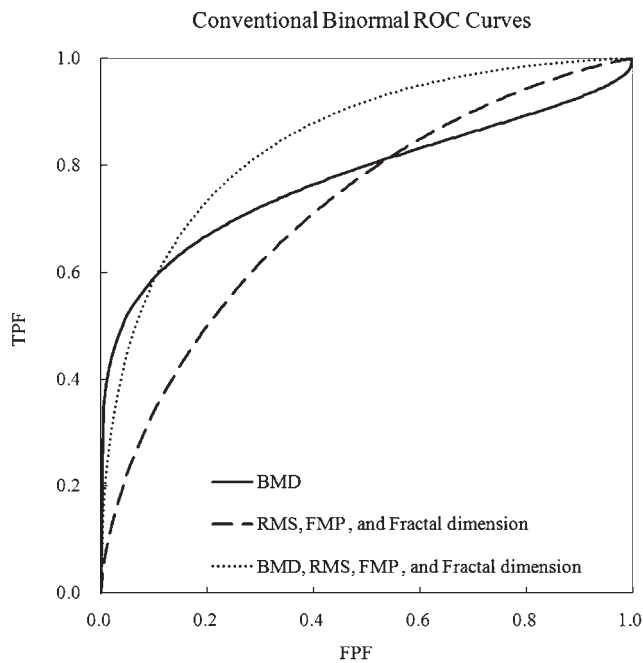


Figure 16. Receiver operating characteristic (ROC) curves indicate the performance of bone mineral density (BMD) measurements, first moment power spectrum (FMP), root mean square (RMS) and fractal dimension to determine the presence or absence of osteoporosis in the spine. The area under the curve (AUC) of BMD was 0.72. The AUC of RMS, FMP and fractal dimension was 0.78. The AUC of BMD, RMS, FMP and fractal dimension was 0.85. FPF, false positive fracture; TPF, true positive fracture.

osteoporosis was in progress, the total amount of microtrabecular pattern was decreased. In the case of CT, a scan series included many slice images; therefore, each slice image included a different amount of microtrabecular pattern. It meant that there was large variation among the images in CT.

These differences among the slices caused the overall differences in fractal dimension (Figure 12). In low-RMS group, RMS had a moderate negative correlation with fractal dimension, whereas RMS had only a weak negative correlation in the high-RMS group.

The results in this study were different from those in the previous study by Caligiuri et al [10], who used a simple lateral spine image. The simple lateral spine image is the X-ray projection images in one direction.

However, CT images showed different bone architecture in each slice. Therefore, the results of this study showed a different tendency from the previous study.

FMP had a strong correlation with fractal dimension. As FMP increased, the fractal dimension also increased (Figure 15). In the low-RMS group FMP had a moderate correlation with fractal dimension, and in the high-RMS group FMP had a weak correlation. This result indicated the strong possibility of osteoporosis.

RMS meant the magnitude of texture pattern. The decrease of RMS resulted in a washed-out image caused by the decrease of bone architecture in osteoporotic bone. According to Caligiuri et al [10], low RMS indicated a fracture or other disease in the spine. FMP, the power spectrum of RMS, included the measurement of the spatial frequency regarding the bone architecture pattern. It meant that high FMP indicated the thinner bone due to fracture or osteoporosis. Large variation in fractal dimension, RMS and FMP meant an acceptable correlation.

According to Katsuragawa et al [19], Caligiuri et al [21] and this study, the collapse of the microtrabecular pattern caused the increase in RMS. As a result, RMS, FMP and fractal dimension were shown as high values (Figures 12–15). High RMS values indicate that these will be more likely to develop into a fracture in future.

In Figure 16, the ROC curve shows the performance of BMD, FMP, RMS and fractal dimension in osteoporosis diagnosis. ROC curves were analysed using LABROC [25–27]. In the case of using only BMD, the AUC was 0.78. When RMS, FMP and fractal dimension were used, the AUC was 0.72. The AUC was 0.85 using all of the factors—BMD, RMS, FMP and fractal dimension. The difference between the cases using three parameters (RMS, FMP and fractal dimension) and those using all parameters (RMS, FMP, fractal dimension and BMD) was significant at the $p=0.05$ level, as determined with a two-tailed test of significance.

Table 1 indicates the diagnostic performance of BMD, FMP, FMS and fractal dimension in osteoporosis.

Of all methods, the WHO has defined BMD as the gold standard. For diagnosis of osteoporosis with BMD, the sensitivity was 44.2% (23/52) with a specificity of 95.2% (40/42; Table 1). Deformation due to osteoporosis in the spine or an increased BMD value due to compression fractures can result in some incorrect diagnoses (7/92). When using RMS, FMP and fractal dimension to diagnose osteoporosis, the sensitivity was 91.4% (5/58)

Table 1. Performance of BMD measurements, FMP, RMS and fractal dimension values to determine the presence or absence of osteoporosis and compression fracture in the spine

Parameter	BMD	RMS, FMP and fractal dimension	BMD, RMS, FMP and fractal dimension
Osteoporosis			
True-positive	23	17	22
True-negative	2	5	3
False-positive	29	16	12
False-negative	40	53	58
Compression fracture			
True-positive	None	6	6
True-negative	7	1	1
False-positive	None	None	None
False-negative	85	85	85

BMD, bone mineral density; FMP, first moment power spectrum; RMS, root mean square.

with a specificity of 50.0% (17/34). When using BMD, the sensitivity was higher than using other factors, while the specificity was lower. This resulted from the database from which compression fracture cases were excluded.

All 92 cases were supposed to exclude the case of compression fracture, but, when using RMS, FMP and fractal dimension together, 6 cases of compression fracture were detected additionally. Compression fractures could not be detected with BMD only, while it could be diagnosed by using RMS, FMP and fractal dimension together.

However, in the case of osteoporosis, the detection ratio was far better using BMD. When using RMS, FMP, fractal dimension and BMD together the result was improved, showing a sensitivity of 64.7% and a specificity of 95.1%. In this case, the ROC curve was also improved (AUC=0.82) compared with the data analysed using only BMD (AUC=0.78) or using RMS, FMP and the fractal dimension (AUC=0.72).

Conclusion

In the case of osteoporosis or osteopenia, using BMD was found to be an effective method for detection; however, in the case of compression fracture in the vertebra, using BMD was found to be less effective because increased BMD can result in an incorrect diagnosis. Applying three parameters (RMS, FMP and fractal dimension) was shown to be a useful method to diagnose compression fracture, while using BMD only was less useful for diagnosis in compression fracture. Therefore, it can be more useful to apply two methods together—both using BMD only and using three parameters (RMS, FMP and fractal dimension)—to diagnose osteoporosis and compression fracture.

For more effective application, additional study of more cases and data will be required.

References

- World Health Organization. Assessment of fracture risk and its application to screening for postmenopausal osteoporosis. Report of a WHO Study Group. Geneva, Switzerland: World Health Organization; 1994.
- World Health Organization. Prevention and management of osteoporosis. Report of a WHO Scientific Group. Geneva, Switzerland: World Health Organization; 2003.
- Kanis JA, Delmas P, Burckhardt P, Cooper C, Torgerson D. Guidelines for diagnosis and management of osteoporosis. *Osteoporos Int* 1997;7:390–406.
- Kanis JA, Glüer CC. An update on the diagnosis and assessment of osteoporosis with densitometry. *Osteoporos Int* 2000;11:192–202.
- Cherian RA, Haddaway MJ, Davie MW, McCall IW, Cassar-Pullicino VN. Effect of Paget's disease of bone on areal lumbar spine bone mineral density measured by DXA, and density of cortical and trabecular bone measured by quantitative CT. *Br J Radiol* 2000;73:720–6.
- Gregson CL, Tobias JH. Interpretation of high bone mineral density measurements. *Osteoporos Rev* 2007;15:2–6.
- Diamond T, Smith A, Schnier R, Manoharan A. Syndrome of myelofibrosis and osteosclerosis: a series of case reports and review of the literature. *Bone* 2002;30:498–501.
- Manganelli P, Giuliani N, Fietta P, Mancini C, Lazzaretti M, Pollini A, et al. OPG/RANKL system imbalance in a case of hepatitis C-associated osteosclerosis: the pathogenetic key? *Clin Rheumatol* 2005;24:296–300.
- Itami Y, Ohata Y. Epidemiology and clinical findings of osteoporosis. *J Jpn Orthop Assoc* 1964;38:487–9.
- Caligiuri P, Giger ML, Favus M. Multifractal radiographic analysis of osteoporosis. *Med Phys* 1994;21:503–8.
- Takigawa A, Ishida T, Yamashita K. Spectral analysis of trabecular patterns. Fundamental experiments and simulations. *Jpn J Radiol Technol* 1991;47:1659–69.
- Ishida T, Yamashita K, Takigawa A. Spectrum analysis of trabecular patterns. *Med Imaging Inform Science* 1992;9:32–49.
- Ishida T, Yamashita K, Takigawa A, Kariya K, Itoh H. Trabecular pattern analysis using fractal dimension. *Jpn J Appl Phys* 1993;32:1867–71.
- Nishihara S, Fujita H, Iida T, Takigawa A, Hara T, Zhou X. Evaluation of osteoporosis in X-ray CT examination: a preliminary study for an automatic recognition algorithm for the central part of a vertebral body using abdominal X-ray CT images. *Comput Med Imag Graph* 2005;29:259–66.
- Dougherty G, Henebry GM. Lacunarity analysis of spatial pattern in CT images of vertebral trabecular bone for assessing osteoporosis. *Med Eng Phys* 2002;24:129–38.
- Ito M, Ikeda K, Nishiguchi M, Shindo H, Uetani M, Hosoi T, et al. Multi-detector row CT imaging of vertebral microstructure for evaluation of fracture risk. *J Bone Miner Res* 2005;20:1828–36.
- Issever AS, Link TM, Kentenich M, Rogalla P, Schwieger K, Huber MB, et al. Assessment of trabecular bone structure using MDCT: comparison of 64- and 320-slice CT using HR-pQCT as the reference standard. *Eur Radiol* 2010;20:458–68.
- Duan Y, Seeman E, Turner CH. The biomechanical basis of vertebral body fragility in men and women. *J Bone Miner Res* 2001;16:2276–83.
- Katsuragawa S, Doi K, MacMahon H. Image feature analysis and computer-aided diagnosis in digital radiography: detection and characterization of interstitial lung disease in digital chest radiographs. *Med Phys* 1988;15:311–19.
- Geoff D. Digital image processing for medical applications. Cambridge, UK: Cambridge University Press; 2009.
- Caligiuri P, Giger L, Favus M, Jia H, Doi K, Dixon LB. Computerized radiographic analysis of osteoporosis. *Radiology* 1993;186:471–4.
- Peitgen H-O, Jürgens H, Saupe D. Fractals for the classroom. Part one: introduction to fractals and chaos. New York, NY: Springer Verlag; 1992.
- Matsufuji N, Tomura H, Futami Y, Yamashita H, Higashi A, Mihohara S, et al. Relationship between CT number and electron density, scatter angle and nuclear reaction for hadron-therapy treatment planning. *Phys Med Biol* 1998;43:3261–75.
- R Foundation Core Team. R: a language and environment for statistical computing. Vienna, Austria: R Foundation for Statistical Computing; 2008.
- Metz CE, Herman BA, Shen J-H. Maximum-likelihood estimation of receiver operating characteristic (ROC) curves from continuously-distributed data. *Stat Med* 1998;17:1033–53.
- Dorfman DD, Alf E. Maximum likelihood estimation of parameters of signal detection theory and determination of confidence intervals rating method data. *J Math Psychol* 1969;6:487–96.
- Grey DR, Morgan BJT. Some aspects of ROC curve-fitting: normal and logistic models. *J Math Psychol* 1972;9:128–39.